Solution adaptive direct variational grids for fluid flow calculations

Article *in* Journal of Computational and Applied Mathematics · March 1996

DOI: 10.1016/0377-0427(95)00017-8

2 authors:

Jose E. Castillo
San Diego State University
202 PUBLICATIONS **1,595** CITATIONS

SEE PROFILE

Erik Morre Pedersen
Aarhus University Hospital
221 PUBLICATIONS **7,833** CITATIONS

SEE PROFILE


ELSEVIER

Journal of Computational and Applied Mathematics 67 (1996) 343–370

JOURNAL OF COMPUTATIONAL AND APPLIED MATHEMATICS

Solution adaptive direct variational grids for fluid flow calculations

José Castillo[a,*], Erik M. Pedersen[b]

[a] *Department of Mathematical Sciences, Interdisciplinary Research Center, San Diego State University, San Diego, CA 92182-0314, United States*

[b] *Rohr Inc., 780 Bay Blvd, Mail Zone 886, Chula Vista, CA 91910, United States*

Received 9 June 1994; revised 10 November 1994

Abstract

In the present study, the discrete variational (DV) grid generation method is used to produce suitable two dimensional grids for solving the inviscid Euler equations for transonic flow past an airfoil. Through the use of a reference grid, the DV method provides excellent control over grid line clustering in the interior of the grid while maintaining smoothly varying grid line distributions. A solution adaptive grid procedure has been developed using the DV approach which re-distributes the existing grid points in order to resolve regions of high flow (solution) gradients. The grid point re-distribution is governed by the principle of equidistribution. The adaption procedure is done by creating an adapted reference grid which is used to drive the grid point re-distribution. Results for transonic flow past an airfoil are presented to demonstrate the feasibility of the DV-reference grid approach.

Keywords: Grid generation; Solution adaption; Reference grid

AMS classification: 65F10; 65N99

1. Introduction

Advances in computational fluid dynamics (CFD) have created the opportunity to analyze fluid flow problems that have increasingly complex physics and geometries. In many such problems there exist regions of both subsonic and supersonic flow, which can include various flow phenomena such as shock waves, boundary layers, free shear layers, flow separation and re-circulation zones. These flow phenomena are characterized by rapidly changing flow variables which result in regions of large solution gradient and/or curvature. The difficulty encountered in solving these types of complex flow problems on a fixed or "non-adaptive" grid is that the grid points must be distributed in the physical region before the solution is known. In most cases, the exact location of these regions is not known a priori, and as a result, the initial grid may not accurately capture all the salient features of the flowfield.

* Corresponding author. E-mail: castillo@myth.sdsu.edu.

SSDI 0377-0427(95)00017-8

Efficient and accurate flowfield calculations require that the computational grid not only resolve the geometrical details of the physical configuration but regions of large solution variation as well. The accuracy of discrete solutions strongly depends on the local grid spacing and the resolution of solution gradients. Therefore, high density grids are needed in regions of large solution variation and relatively coarse grids are needed in regions of small solution variation. Adaptive grid generation techniques are used to adapt the grid point distribution during the solution process in order to resolve regions of large solution variation. Adaptive grids are used to improve the efficiency and accuracy of the numerical calculations as well as to resolve the details of the local physics.

As in the variational methods described by Brackbill and Saltzman [5] and Roache and Steinberg [24], the discrete variational (DV) method controls three properties of the grid: the spacing between the grid lines (smoothness), the area of the grid cells, and the orthogonality of the grid lines. In the variational approach the minimization problem is frequently solved by calculating the Euler–Lagrange equations for each functional (see [18] for a detailed explanation). The resulting Euler–Lagrange equations form a system of partial differential equations which is usually solved using standard finite-difference algorithms. This problem is generally costly to solve. In the direct approach the functionals are discrete, are defined directly over the grid, and the minimization part is a less expensive problem.

This method belongs to a general family of direct optimization grid generation methods [9, 16]. The grid is generated by solving a minimization problem resulting from a weighted combination of three functionals, each representing one of the grid properties to be controlled:

$$\text{Minimize } F = aF_S + bF_A + cF_O \quad (a, b, c \geqslant 0), \tag{1.1}$$

where F_S, F_A, and F_O are the length, area, and orthogonality functionals, respectively and a, b, c are the functional scaling factors. The resulting minimization problem (1.1) is solved using a conjugate gradient iterative method. This minimization problem could be very large even for problems that are considered of modest size for aerodynamics calculations [15].

The DV method has been successfully used to produce grids on many two-dimensional model regions [7, 8, 10]. The DV method has been shown to produce grids nearly identical to those produced by the Roache and Steinberg [24] formulation, however, the DV method is considerably faster than theirs [6].

Many different solution adaptive techniques have been developed and implemented based on the re-distribution approach. Most of these adaptive grid procedures attempt to re-distribute the grid points in order to equally distribute some measure of the solution error over the field, however, each differs in its individual approach. The most popular approach has been to maintain a constant product of a weighting function, which is proportional to an error measure, and the grid interval throughout the solution domain. Benson and McRae [4] and Abolhassani and Smith [1] used a linear combination of the gradients of several dependent flow variables to define the weight function. Harvey et al. [14] used a linear combination of the gradients and curvature of the dependent and/or physical flow variables as the error measure. In the method developed by Harvey et al. [14] the grid movement is controlled by forces analogous to tensional and torsional spring forces with the spring constants set equal to the weighting functions. Kim and Thompson [17] and Anderson [2] have developed adaptive grid control functions that are related to the changes in the dependent flow variables so that the Poisson grid generation system [26] can be used as an

adaptive scheme. Also, Roache et al. [23] developed an adaptive hybrid Poisson algorithm. Lee and Loellbach [19, 20] use a parametric mapping between the physical grid and the computational grid for the re-arrangement of grid points to adapt to solution gradients. The mapping functions are influenced by the effects of grid control sources which are extracted from the distribution of the flow variables. Shyy [25] utilizes multiple one-dimensional adaptions along fixed coordinate lines to produce adaptive grids for improved Navier–Stokes flow calculations.

The first part of this paper presents suitable two-dimensional initial grids for solving the Euler/Navier–Stokes equations for transonic flow past an airfoil using the DV grid generation method. Examples of O-type and C-type grids will be presented. The second part presents the use of a solution-adaptive grid generation procedure using the DV approach, which adapts the grid point distribution to resolve regions of high solution gradients. A unique feature of this paper is the use of a reference grid to move the grid with the solution.

The adaptive procedure incorporated in the present study re-distributes the existing grid points to cluster in regions of high solution gradients. The grid point re-distribution is based on the equidistribution principle wherein the product of the grid spacing and a specified weight function is constant over the field. The weight function is defined such that the grid points will adapt to the gradients of any specified flow quantity.

Results for transonic flow past an airfoil are presented in order to demonstrate the improvement obtainable with this solution adaptive grid procedure.

This paper clearly demonstrates the feasibility of the DV-reference grid approach. Further studies are needed to determine in what situations this method may be superior. In particular extensions to three-dimensional problems are in progress.

2. Problem description

2.1. Airfoil problem

This relatively simple, two-dimensional example of transonic flow past an airfoil illustrates the need for a solution-adaptive grid procedure. Even if only an inviscid Euler solution is required, the computational grid must resolve the high flow acceleration region around the leading edge as well as the high streamwise gradients through the shocks. However, the exact location and strength of the shocks are not known a priori. Depending on the onset flow conditions (M_∞, angle of attack α), these shocks can potentially exist anywhere from about the midpoint of the chord to the trailing edge. If a range of onset conditions needs to be analyzed, a large number of grid points are required to adequately resolve the leading edge gradients as well as the shocks located anywhere aft of the midpoint of the chord. A solution-adaptive grid procedure is required to efficiently utilize the least number of grid points to resolve both the leading edge gradients as well as the shocks.

2.2. Global adaptive procedure

The following solution adaptive procedure has been implemented. Generate an initial grid based on the geometry and anticipated flowfield characteristics using the DV method. Obtain a

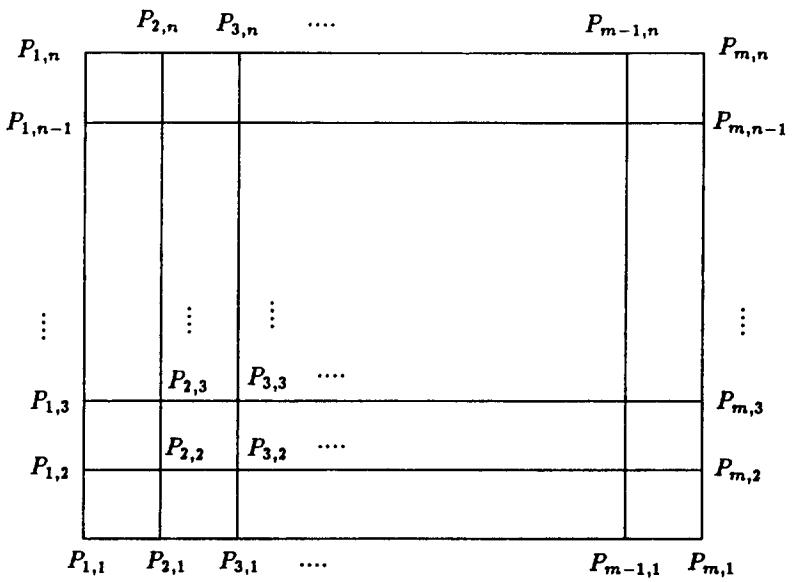

Fig. 1. A rectangular region.

converged flowfield solution on the initial grid using the PARC Euler/Navier–Stokes code [13]. Adapt the grid point distributions to resolve regions of high solution gradient that are present in the initial solution field. Obtain a converged flowfield solution on the adapted grid and evaluate the results. This procedure is summarized in the following steps.

Step 1: Generate initial grid.
Step 2: Compute flow solution on initial grid.
Step 3: Generate solution-adapted grid.
Step 4: Compute flow solution on adapted grid.
Step 5: Evaluate results, go to Step 3 if required.

The grid generation algorithm and the solution adaptive algorithm will be described briefly in the following sections. The PARC code is utilized as a "black box" flow solver in the present study. This particular flow solver was selected because of its versatility and one of the author's experience with the code as a user. The general features of the PARC code are outlined in the following section.

2.3. *Flow solver*

The PARC code [13] is a general purpose Euler/Navier–Stokes solver developed by Sverdrup Technology, Inc. It is based on the NASA Ames ARC code [24] and has been extensively enhanced for usage in an applications oriented environment. It can simulate a wide variety of flows, including those with complex geometries and complex fluid dynamics. The computational domain may be decomposed into blocks in order to simplify the grid generation process. Inviscid or viscous flows can be calculated. Viscous flows may be treated as laminar or turbulent. The PARC code is available in a two-dimensional/axisymmetric version and a fully three-dimensional version. The two-dimensional version was used in the present study.

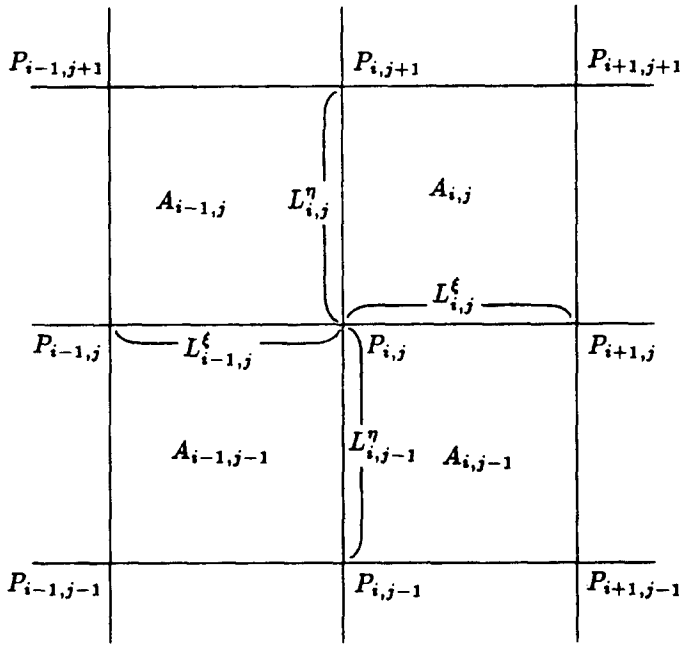

Fig. 2. Grid segment and cell area definition.

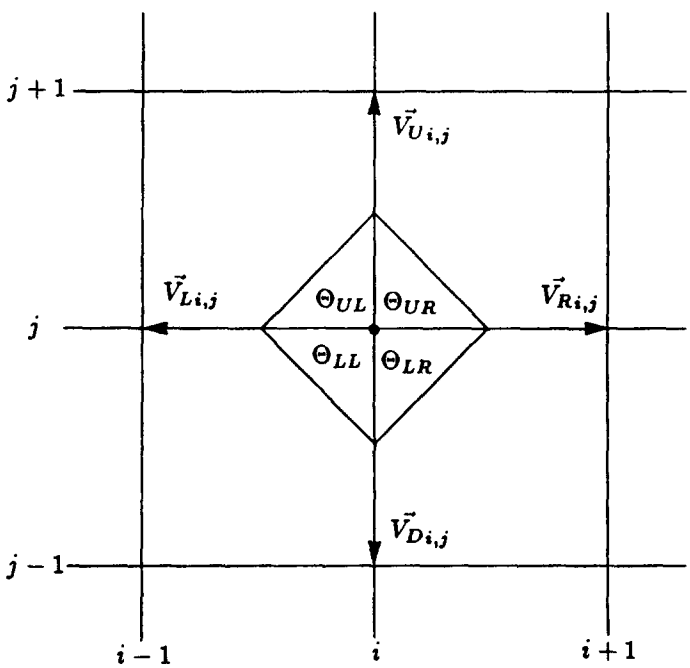

Fig. 3. Grid angle definition.

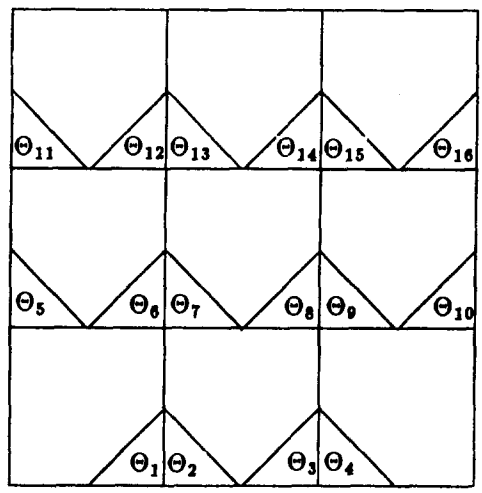

Fig. 4. A 4×4 example of all upper angles.

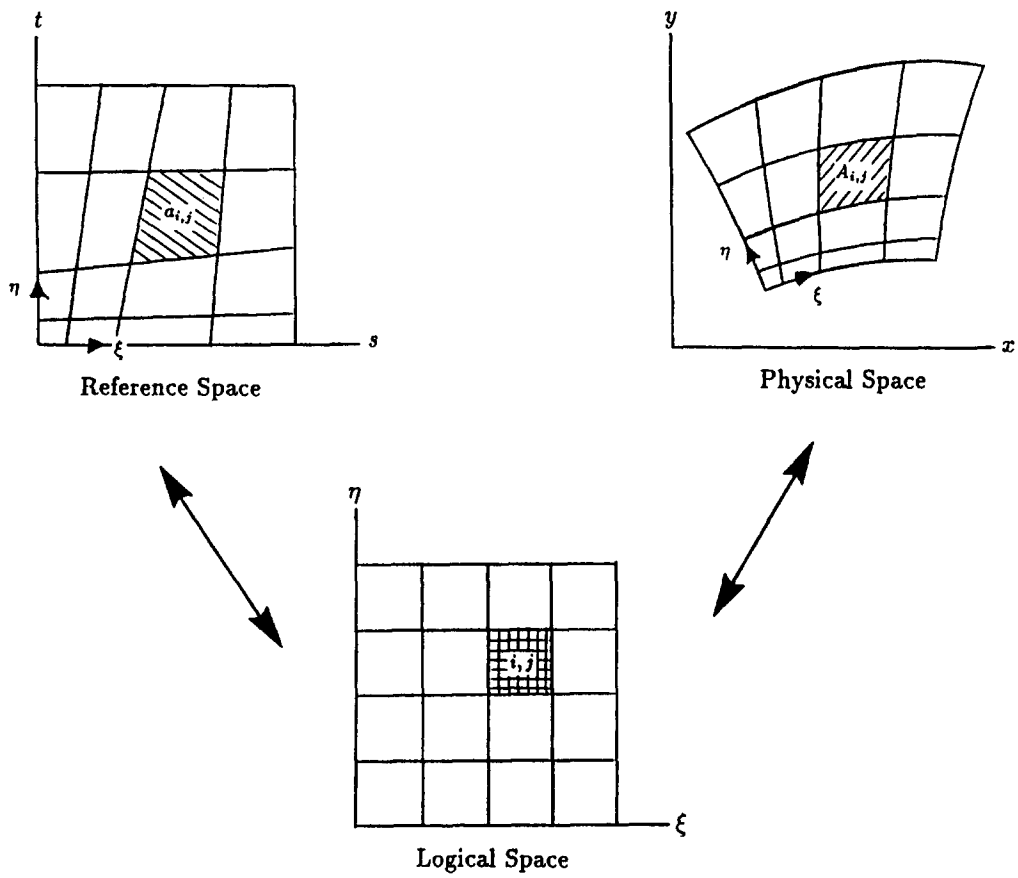

Fig. 5. Relationship between physical space, reference space, and logical space.

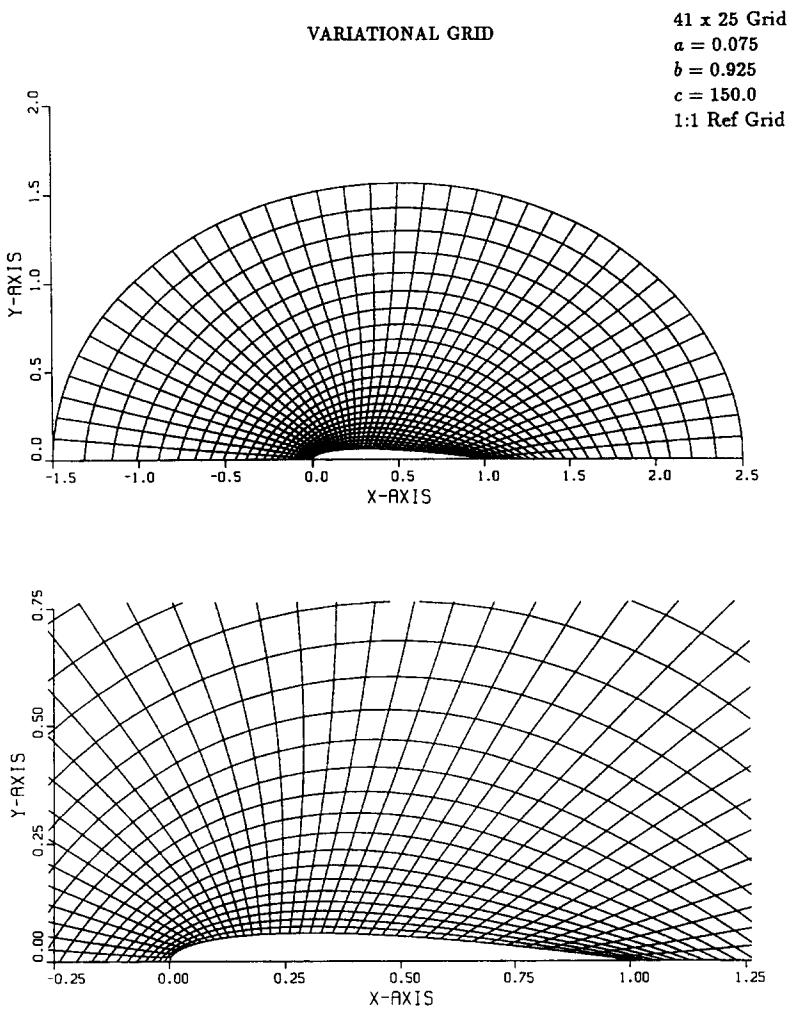

Fig. 6. Discrete variational grid: O-type grid (upper half).

The Beam and Warming approximate factorization algorithm [3] is the basis of the steady-state solution scheme of the PARC code. This algorithm is an implicit scheme that solves the set of equations produced by central-differencing the time-dependent form of the Navier–Stokes equations on a structured grid. Since these equations are formulated in strong conservation law form for a curvilinear set of coordinates, the resulting algorithm is very general with the desirable features of global conservation and shock capturing [13]. The PARC code was installed and run on the Cray Y-MP at the San Diego Supercomputer Center (SDSC).

3. Grid generation

The DV method [6–8] controls three properties of the grid: the spacing between the grid lines (smoothness), the area of the grid cells, and the orthogonality of the grid lines (see Figs. 1–4). The

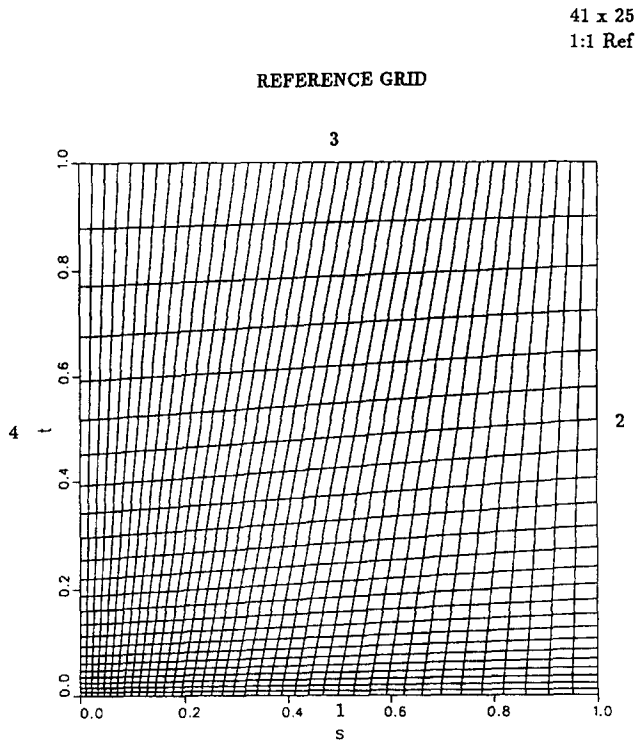

Fig. 7. 1:1 reference grid: O-type grid (upper half).

grid is generated by solving a minimization problem resulting from a weighted combination of three functionals, each representing one of the grid properties to be controlled:

$$\text{Minimize } F = aF_S + bF_A + cF_O \quad (a, b, c \geqslant 0), \tag{3.1}$$

where F_S, F_A, and F_O are the length, area, and orthogonality functionals respectively and a, b, c are the functional scaling factors.

The length functional will be described in detail to illustrate the grid generation method.

3.1. *Length functional* F_S

The length functional (F_S) is used to control the spacing between the grid lines and is defined as the sum of the horizontal and vertical length functionals:

$$F_S = S_H + S_V,$$

where the horizontal and vertical length functionals, S_H and S_V, are given by:

$$S_H = \sum_{i=1}^{m-1} \sum_{j=2}^{n-1} (L_{i,j}^{\xi})^2, \tag{3.2a}$$

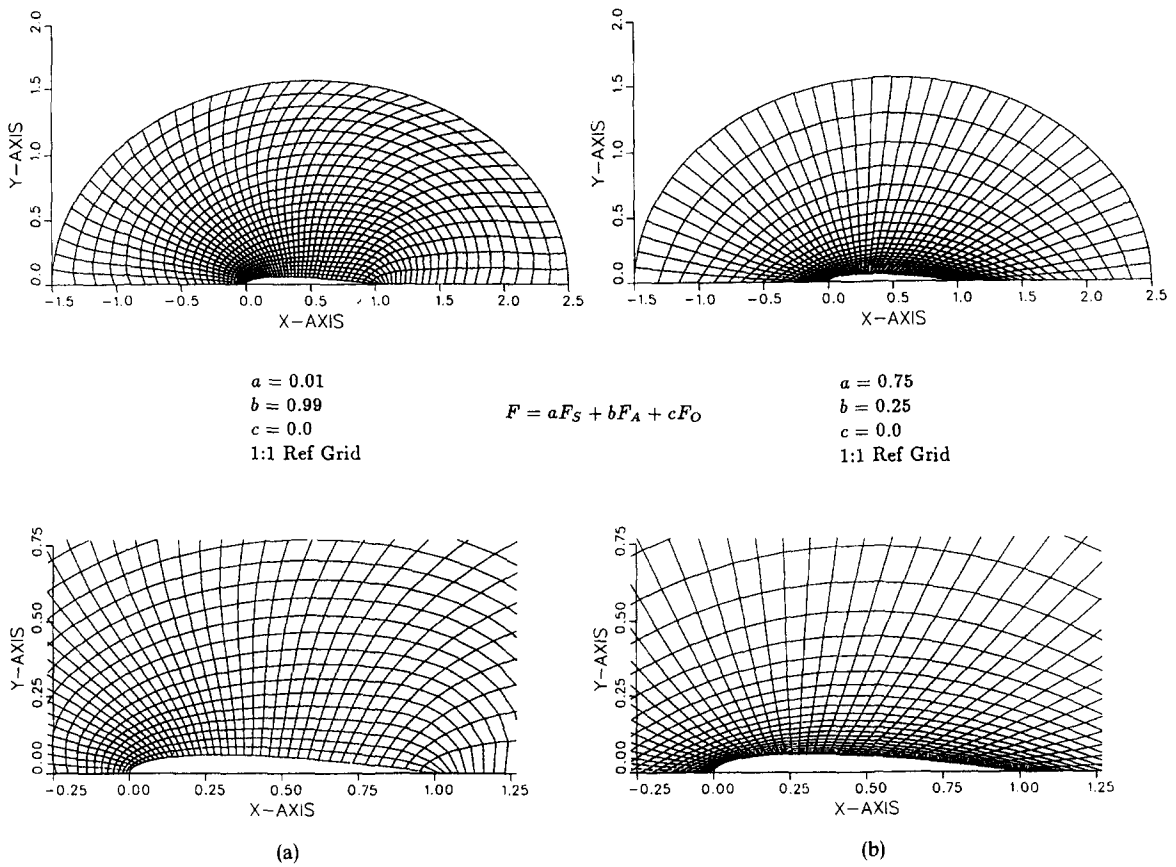

Fig. 8. (a) Effects of too much weighting on the area functional and not enough on the length functional. (b) Effects of too much weighting on the length functional and not enough on the area functional.

$$S_V = \sum_{i=2}^{m-1} \sum_{j=1}^{n-1} (L_{i,j}^{\eta})^2 . \tag{3.2b}$$

$L_{i,j}^{\xi}$ and $L_{i,j}^{\eta}$ are defined as the lengths of the i,jth logical "horizontal" (ξ) and logical "vertical" (η) grid segments in physical (x, y) space, respectively (see Fig. 5).

3.2. *Reference grid*

In order to obtain more refined control over the properties of the grid, the concept of a reference grid is used [10, 11, 23]. The reference grid is a grid which is much simpler than the physical grid but has the same general properties. In most cases the physical region is rather complex, therefore we define another region, called the reference region, which is considerably simpler than the physical region (either a rectangle or simply the unit square).

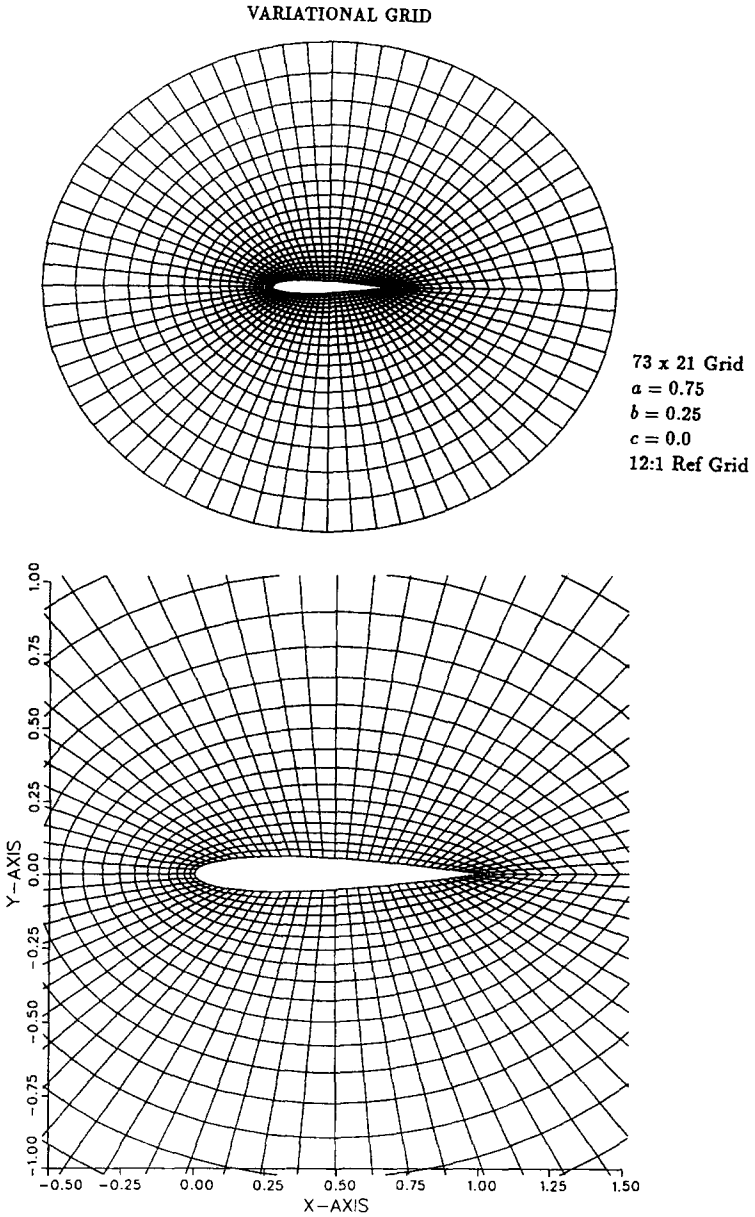

Fig. 9. Discrete variational grid: O-type grid.

On this reference region we define a grid which has the general properties which are desired on the physical grid (e.g., grid point clustering in certain regions). As shown in Fig. 5, there is a one-to-one correspondence between the reference grid and the physical grid, in other words, for each grid segment or grid cell in physical space there is a corresponding grid segment or grid cell in reference space.

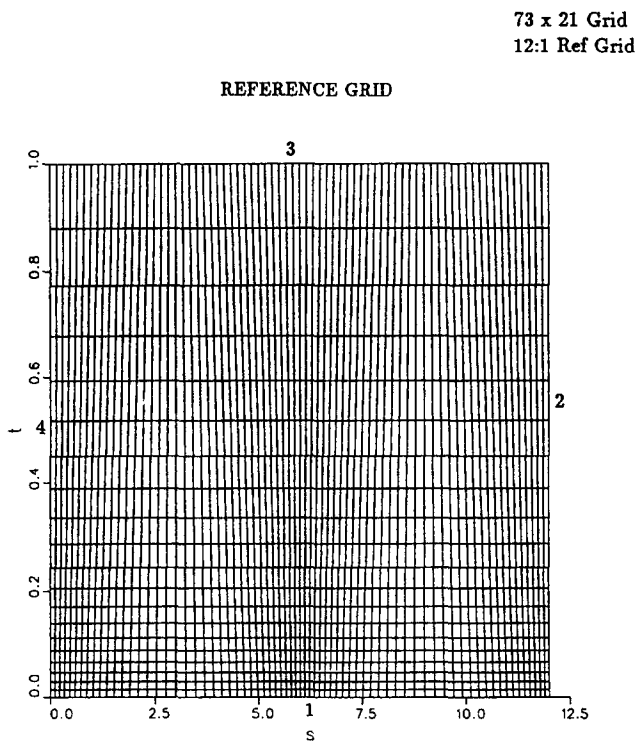

Fig. 10. 12:1 reference grid: O-type grid.

For notation purposes let $p_{i,j} = (s_{i,j}, t_{i,j})^t$ be the i,jth point in reference space, where $1 \leqslant i \leqslant m$, and $1 \leqslant j \leqslant n$. Control over the properties of the physical space grid is accomplished by adding scaling factors (weights), based on the reference grid, to the length and area functionals, F_S and F_A. The reference length weights, $l^{\xi}_{i,j}$ and $l^{\eta}_{i,j}$, are defined as the lengths of the i,jth logical "horizontal" (ξ) and logical "vertical" (η) grid segments in reference (s, t) space.

The reference area weight $a_{i,j}$ is defined as the area of the i,jth grid cell in reference (s, t) space.

The reference length weights $l^{\xi}_{i,j}$, $l^{\eta}_{i,j}$, see Fig. 2, are included in the length functional F_S (3.2) resulting in the "scaled" length functional:

$$F_S = S_H + S_V = \sum_{i=1}^{m-1} \sum_{j=2}^{n-1} \frac{(L^{\xi}_{i,j})^2}{l^{\xi}_{i,j}} + \sum_{i=2}^{m-1} \sum_{j=1}^{n-1} \frac{(L^{\eta}_{i,j})^2}{l^{\eta}_{i,j}} \tag{3.3}$$

A length functional of the form given by (3.3) scale the physical space grid such that the length of the grid segments of the grid cells in physical space are proportional to the corresponding grid segments in reference space.

The folding of numerical grids is strongly influenced by the shape of the physical region and the dimensions of the grid. In the DV approach, the reference grid is used as a tool to prevent such grid folding. Castillo et al. [12] have shown that for certain physical regions, using a unit square

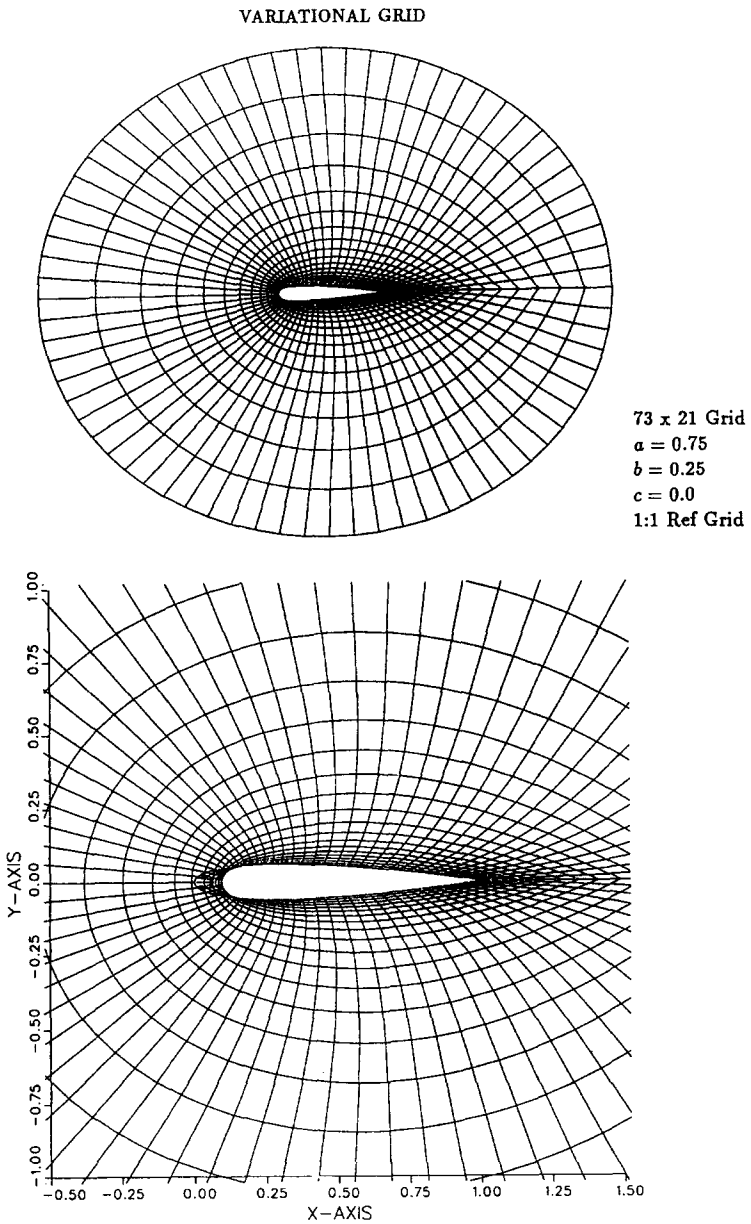

Fig. 11. Example of a folded grid: reference grid stretching effects.

reference grid can produce grids that are folded. By stretching the reference grid into a rectangle whose dimensions more closely approximate the dimensions of the physical region, the grid becomes un-folded and has more acceptable properties. This is an important feature of the reference grid which has been utilized in the present study.

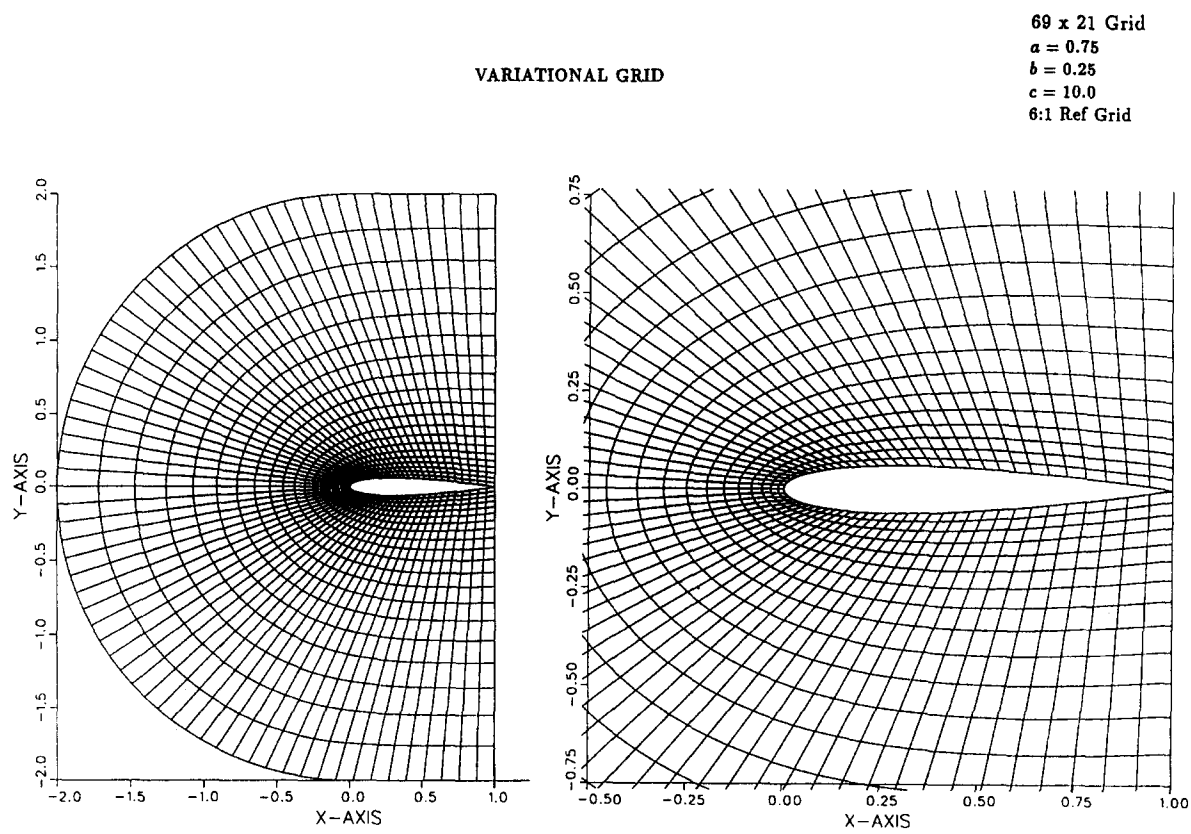

Fig. 12. Discrete variational grid: C-type grid.

4. Results and discussion

The grids presented herein were generated for the purpose of solving the inviscid Euler equations for transonic flow past an airfoil. Therefore, no attempts were made to resolve any viscous flow phenomena, i.e., the boundary layer on the surface of the airfoil.

4.1. *O-type grid (upper half)*

Fig. 6 shows the "best" grid obtained for the upper half O-type grid configuration around a NACA 0012 airfoil. Fig. 7 shows the reference grid utilized to produce the variational grid.

There are 41 grid points along the airfoil surface (ξ direction) and 25 grid points in the radial (η) direction. The boundary geometry for the O-type grid configuration was defined using ROUT = 2.0, and a chord length $C = 1.0$ was used for all configurations. The distribution of grid points on the airfoil surface was defined so as to resolve the anticipated flow gradients around the

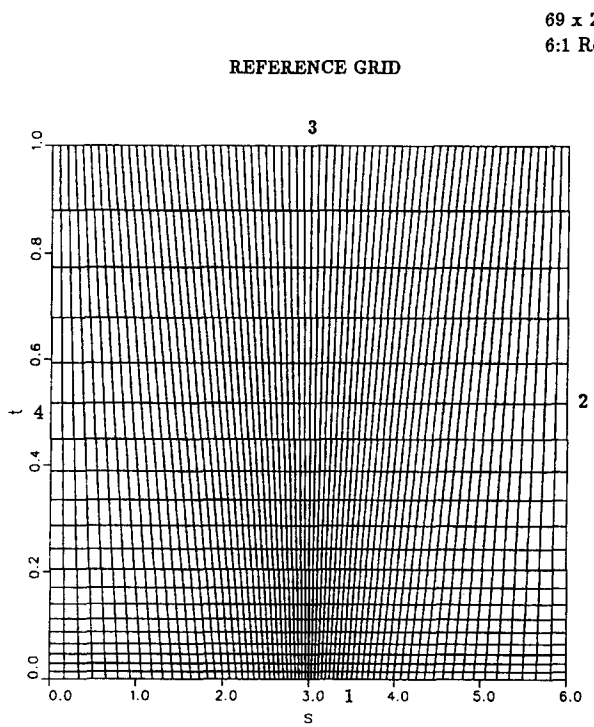

Fig. 13. 6:1 reference grid: C-type grid.

leading edge. The clustering of grid points at the trailing edge of the airfoil was not needed for this configuration. The stretching factors used to define the boundary grid points were; $\alpha_S(1) = 1.04$ on Edge 1 (airfoil surface), $\alpha_S(2) = 1.10$ on Edge 2 (downstream boundary), $\alpha_S(3) = 1.00$ on Edge 3 (outer boundary), and $\alpha_S(4) = 1.13$ on Edge 4 (upstream boundary). The "optimum" scaling factors for the length, area, and orthogonality functionals were found to be $a = 0.075$, $b = 0.925$, and $c = 150.0$, respectively. The reference grid defined on the unit square was found to be adequate for this configuration (see Fig. 7).

The variational grid (Fig. 6) has very good overall qualities, it is very smooth with grid line clustering near the airfoil surface, and has good overall orthogonality along the leading edge of the airfoil and in the field. However, towards the trailing edge of the airfoil the grid becomes quite skewed. A certain amount of skewness is expected in this region because of the O-type grid configuration. This skewness is a result of the orthogonality functional that is not scaled properly (i.e., it tends to provide more orthogonality control where the grid cells are large and less where the grid cells are small). Large grid cell aspect ratios magnify this effect (e.g., near the surface at the trailing edge). In addition, more control is needed over the orthogonality of the grid lines intersecting the boundary, especially on the airfoil surface. Control over boundary orthogonality is required before a Navier–Stokes calculation can be performed. Even with these orthogonality shortcomings, the variational grid is quite acceptable for an inviscid (Euler) flowfield analysis.

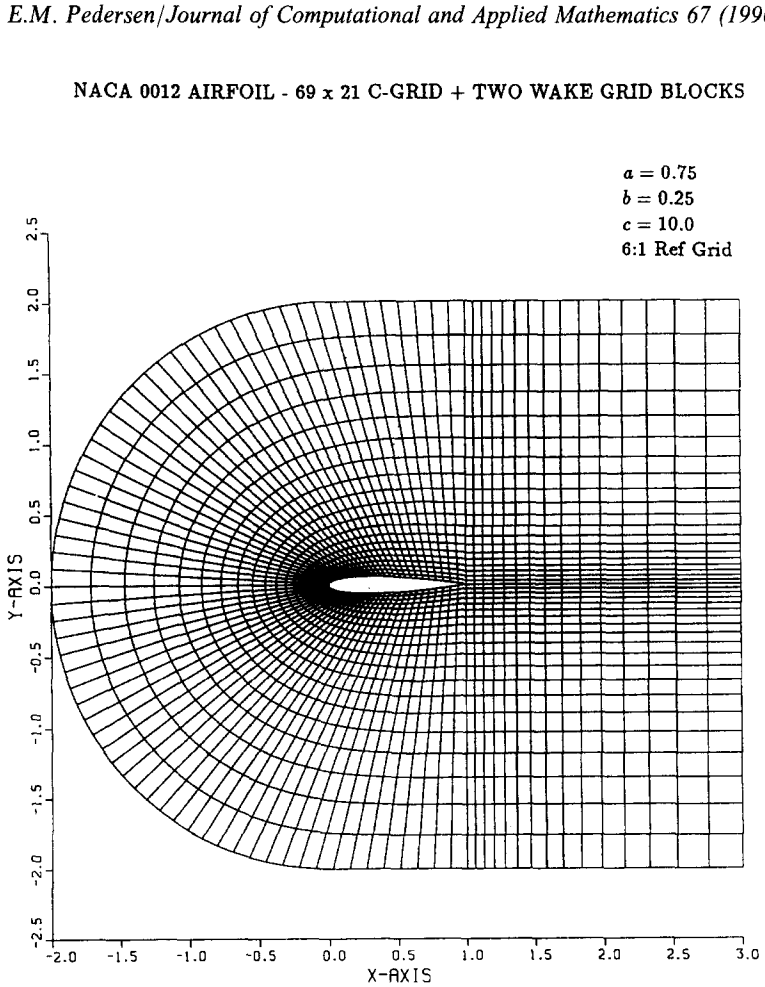

Fig. 14. C-type grid with two wake grid blocks.

For any given grid configuration (i.e., boundary geometry, grid type and size) there is an "optimum" combination of the functional scaling factors (a, b, c) and reference grid stretching factor which produces the "best" variational grid. However, there are currently no methods available to select the "optimum" values for these parameters a priori; the optimum values were determined only after trial and error. Fig. 8 shows the effects of "nonoptimal" subfunctional scaling factors on the half O-grid when the reference grid stretching factor is kept constant. Fig. 8(a) shows the result of too much weighting on the area functional and not enough on the length (smoothness) functional. This produces a grid in which the areas of the grid cells are nearly constant over the region, similar to an algebraic grid generated using transfinite interpolation formulated in logical space. Fig. 8(b) shows the result of too much weighting on the length functional and not enough on the area functional. Notice how the ξ-coordinate lines are severely compressed towards the airfoil surface. This particular characteristic may be valuable for resolving the viscous length scales when

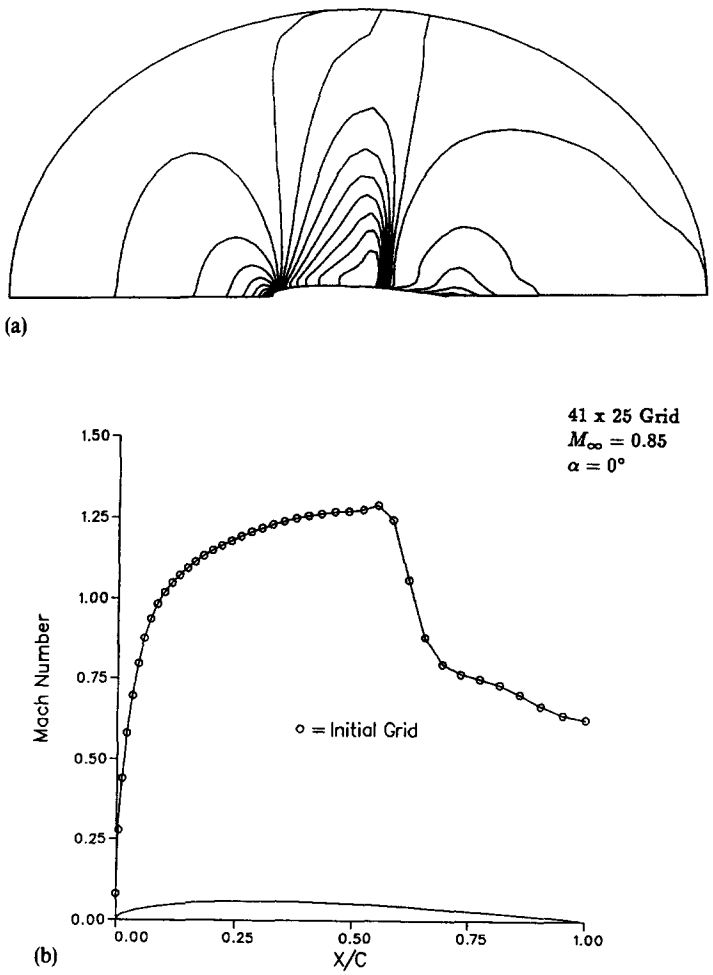

Fig. 15. Inviscid flowfield solution: O-type grid (upper half): (a) flowfield Mach contours; (b) Mach number distribution on airfoil surface.

generating a grid for a viscous Navier–Stokes calculation. Both grids shown in Fig. 8 are considered to be unacceptable for the present analysis.

4.2. O-type grid

Fig. 9 shows the variational grid for the full O-type grid configuration. Fig. 10 shows the reference grid utilized to produce the variational grid.

For the full O-grid, there are 73 grid points along the airfoil surface (ξ direction) and 21 grid points in the radial (η) direction. The boundary geometry for the full O-type grid configuration was defined using ROUT = 2.5. The distribution of grid points on the airfoil surface was defined so as

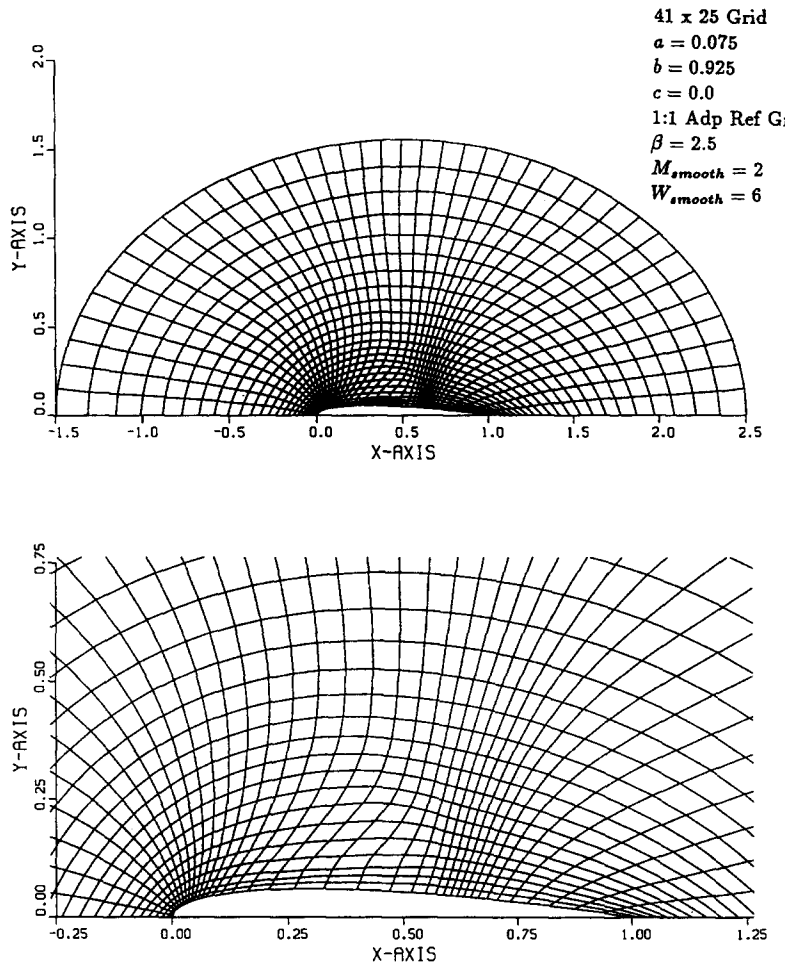

Fig. 16. Adapted grid — 1st adaptive iteration.

to resolve the anticipated flow gradients around the leading edge as well as the trailing edge region. The option of clustering at both the leading and trailing edges was utilized for this configuration. The stretching factors used to define the boundary grid points were: $\alpha_S(1) = 1.05$ on Edge 1 (airfoil surface), $\alpha_S(2) = \alpha_S(4) = 1.12$ on the downstream boundary (both Edges 2 and 4), $\alpha_S(3) = 1.00$ on Edge 3 (outer boundary) The "optimum" scaling factors for the length, area, and orthogonality functionals were found to be $a = 0.75$, $b = 0.25$, and $c = 0.0$, respectively. This configuration required that the reference grid be stretched along the horizontal (s) axis into a 12:1 rectangle (see Fig. 10).

The variational grid for the full O-grid configuration (Fig. 9) again has very good overall qualities, and as expected, has a much smoother coordinate line distribution around the leading

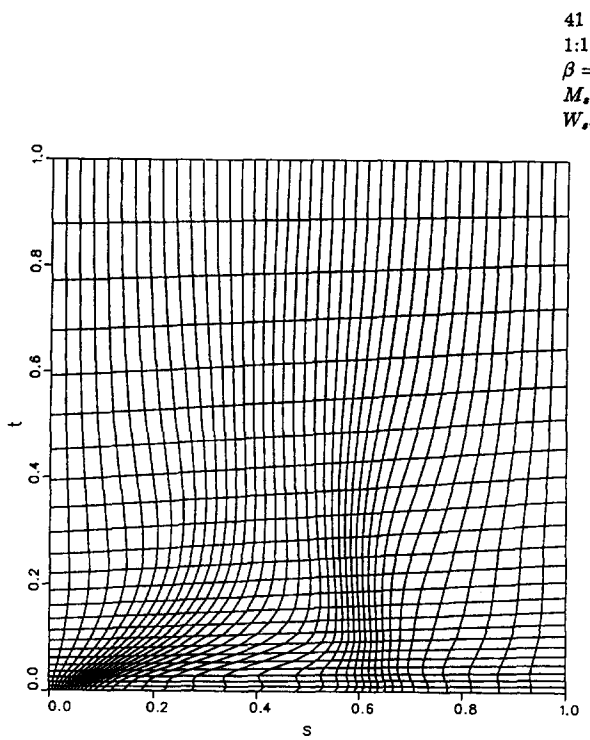

Fig. 17. Adapted reference grid — 1st adaptive iteration.

edge than the half O-grid. The same comments on orthogonality that were stated above for the half O-grid can be applied to the full O-grid as well. However, the orthogonality functional was not used for this configuration (i.e., $c = 0$), because it did not produce any desired properties in the final grid. Again, this variational grid is quite acceptable for an inviscid (Euler) flowfield analysis.

To demonstrate the importance of stretching the reference grid into a rectangle for certain configurations, Fig. 11 has been included. Fig. 11 shows the variational grid for the full O-grid configuration resulting from a unit square reference grid with all the functional scaling factors held constant. Note that the grid around the leading edge is folded. By holding all other factors constant, just stretching the reference grid into a 12:1 rectangle produces an un-folded, acceptable grid, see Fig. 9.

4.3. C-type grid

Fig. 12 shows the variational grid for the C-type grid configuration. Fig. 13 shows the reference grid utilized to produce the variational grid.

For the C-grid, there are 69 grid points along the airfoil surface (ξ direction) and 21 grid points in the radial (η) direction. The boundary geometry for the C-type grid configuration was defined using ROUT = 2.0. The distribution of grid points on the airfoil surface was defined so as to resolve the anticipated flow gradients around the leading edge. The stretching factors used to define the boundary grid points were; $\alpha_S(1) = 1.05$ on Edge 1 (airfoil surface), $\alpha_S(2) = \alpha_S(4) = 1.12$ on the downstream boundaries (both Edges 2 and 4), $\alpha_S(3) = 1.00$ on Edge 3 (outer boundary). The

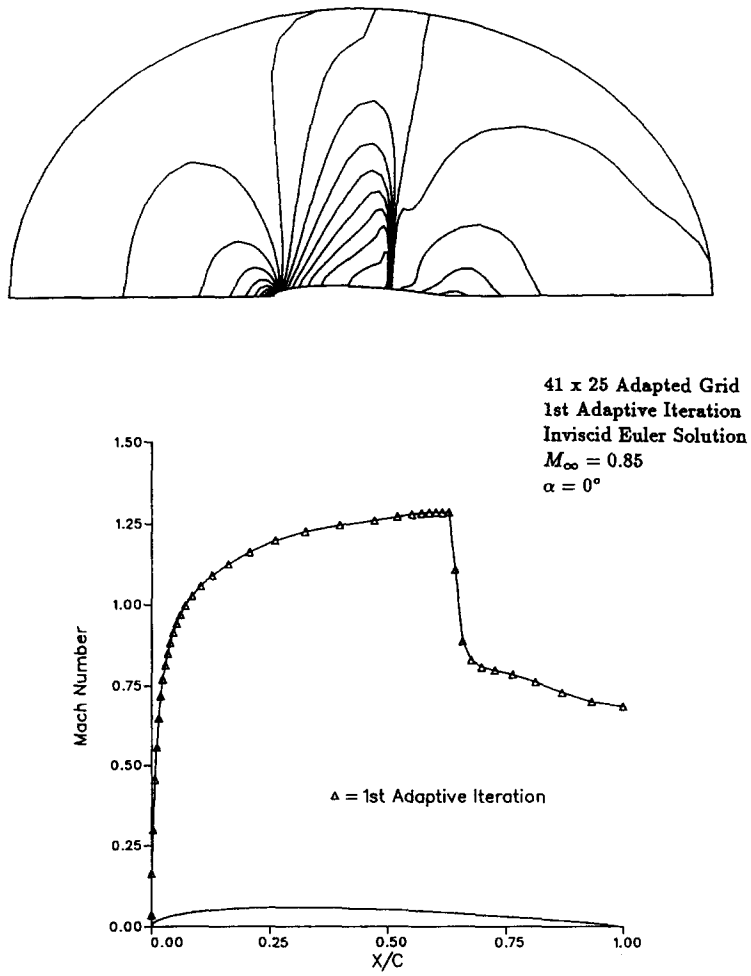

Fig. 18. Converged flowfield solution — 1st adaptive iteration.

"optimum" scaling factors for the length, area, and orthogonality functionals were found to be $a = 0.75$, $b = 0.25$, and $c = 10.0$, respectively. This configuration required that the reference grid be stretched along the horizontal (s) axis into a 6:1 rectangle (see Fig. 13).

The variational grid (Fig. 12) has very good overall qualities, and as expected with the C-grid configuration, has no skewness problems at the trailing edge (downstream boundaries). This variational grid is quite acceptable for an inviscid (Euler) flowfield analysis. Before a flowfield analysis can be performed with the C-grid, two additional wake grid blocks must be defined as shown in Fig. 14.

4.4. Flow solution on the fixed grid

As stated previously, the upper half of the O-type grid (Fig. 6) was chosen for flowfield analysis in order to provide a simple region on which to develop the solution adaptive grid procedure. The

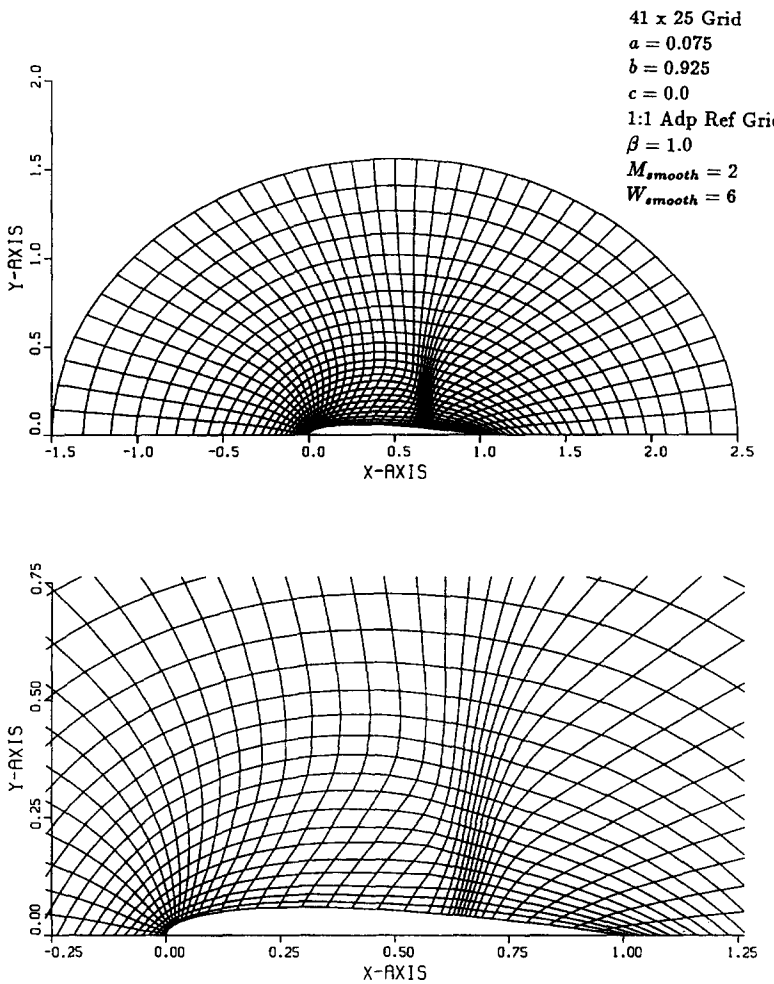

Fig. 19. Adapted grid — 2nd adaptive iteration.

PARC code was used to calculate the two-dimensional, transonic, inviscid flowfield about the symmetry plane of the NACA 0012 airfoil. The onset flow conditions analyzed for the model test case were a freestream Mach number (M_∞) of 0.85 and zero degrees angle of attack ($\alpha = 0°$). Fig. 15 shows the converged flowfield solution for the symmetry plane condition. Fig. 15(a) shows the iso-Mach contours within the field and Fig. 15(b) shows the Mach number distribution on the airfoil surface. Fig. 15 clearly shows the grid resolved the high leading edge gradients that were expected, however, the shock wave has been "smeared" over five grid points which is about 10% of the chord. The resolution of the grid in the region of the shock is obviously inadequate. In order to accurately capture the shock wave, a solution adaptive grid procedure is required to sense the high streamwise gradients through the shock and re-distribute the grid points to resolve these high gradient regions.

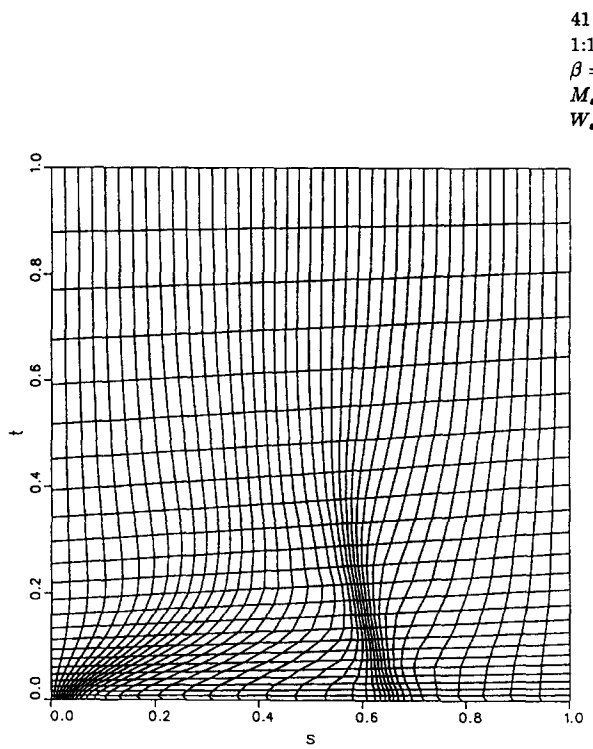

Fig. 20. Adapted reference grid — 2nd adaptive iteration.

5. Solution adaption

The present adaptive technique is based on re-distributing the existing grid points in order to resolve regions of high solution gradients. The grid point re-distribution is governed by the principle of equidistribution wherein the product of the grid spacing and a specified weight function is constant over the field. The adaptive weight function is defined such that the grid points will adapt to the gradient of any specified flow quantity. A significant aspect of our algorithm is that our adaption involves boundary adaption as well as interior grid adaption.

The current adaption procedure is based on a series of multiple one-dimensional adaptions along parametrized curvilinear coordinate lines [11]. The parametrization is defined by transforming the two-dimensional physical space curve (e.g., ξ- or η-coordinate line) into a one-dimensional curve based on normalized arc length. Using this approach, the grid points are constrained to move only along one family of fixed coordinate lines during each adaptive stage.

The adapted grid point distribution along a parametrized coordinate line is obtained by minimizing a one-dimensional adaptive length functional. The adaptive length functional is formulated based on the principle of equidistribution. The adapted parametrized arc length distributions are used to define an adapted reference grid. Reference length and area weights based on the adapted reference grid are used to drive the grid point re-distribution in two-dimensional.

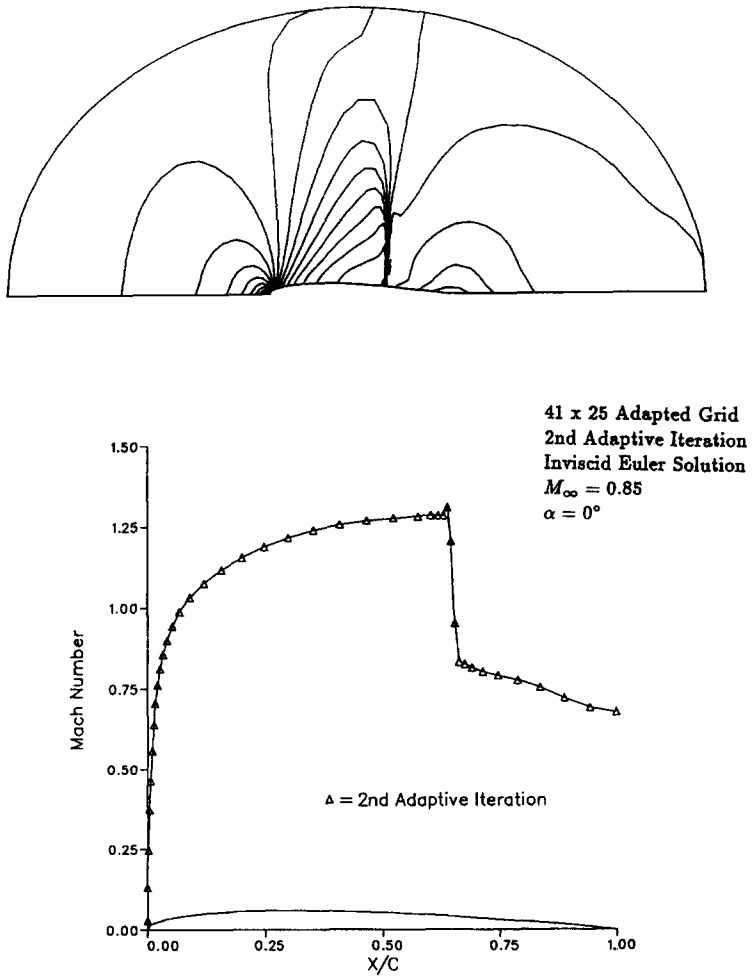

Fig. 21. Converged flowfield solution — 2nd adaptive iteration.

The final two-dimensional adapted grid is obtained by minimizing the length and area functionals given by (3.16) and (3.18) utilizing the adapted reference weights.

The solution adaptive formulation was developed and tested in one dimension and then extended to the two-dimensional problem [21].

5.1. Results – 2-D adapted grids

Fig. 16 shows the adapted physical space grid following the first adaptive iteration. Fig. 17 shows the adapted reference grid utilized to produce the adapted physical space grid. Note that throughout all adaptive iterations the scaling factors for the length and area functionals, a and b, and the reference grid stretching factor are identical to those utilized for the initial grid (i.e., $a = 0.075$, $b = 0.925$, and 1:1 Ref Grid). However, the orthogonality functional scaling factor c was set to

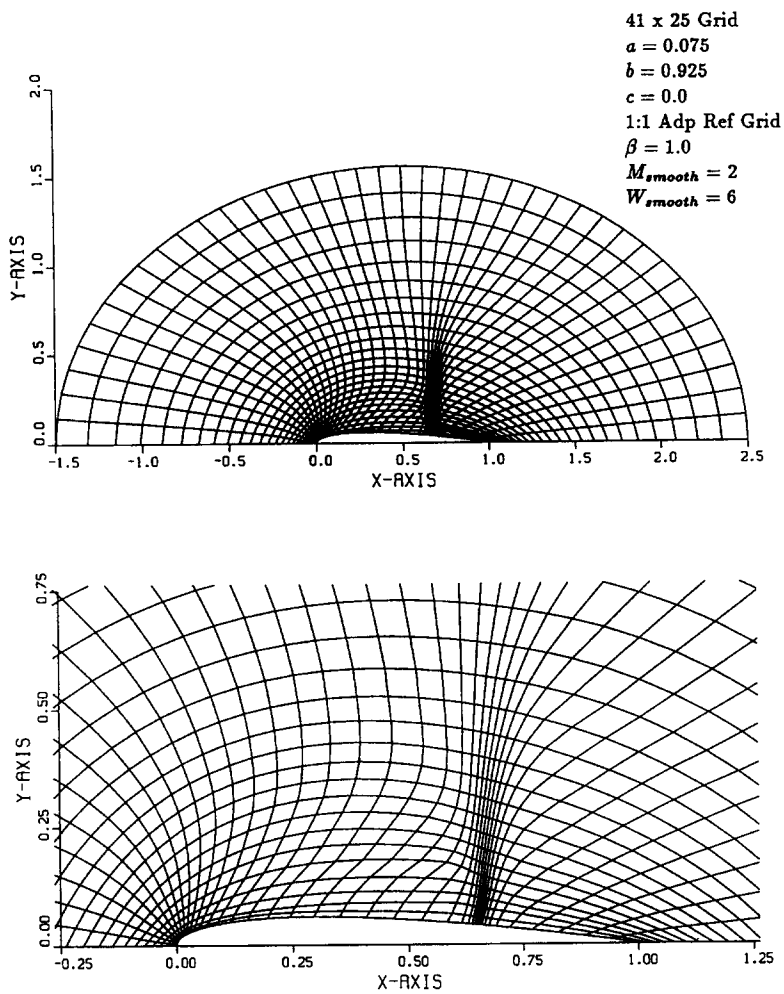

Fig. 22. Adapted grid — 3rd adaptive iteration.

zero. It was found that the orthogonality functional was not needed and was therefore set to zero during all adaptive iterations. The Mach number was selected as the flow quantity whose gradient was used to define the adaptive weights. A gradient scaling factor $\beta = 2.5$ was used for the first adaptive iteration. The Mach number surface has undergone two smoothing iterations ($M_{\text{smooth}} = 2$) while the adaptive weight surface has undergone six smoothing iterations ($W_{\text{smooth}} = 6$). The adapted grid (Fig. 16) shows grid line clustering at the leading edge and in the vicinity of the shock wave without any regions becoming devoid of points. The resulting grid is quite smooth with good overall orthogonality, even without utilizing the orthogonality functional. Fig. 18 shows the converged flowfield solution on the adapted grid following the first adaptive iteration. Fig. 18 shows that the shock discontinuity is captured much more sharply on the adapted grid than on the initial grid (Fig. 15)

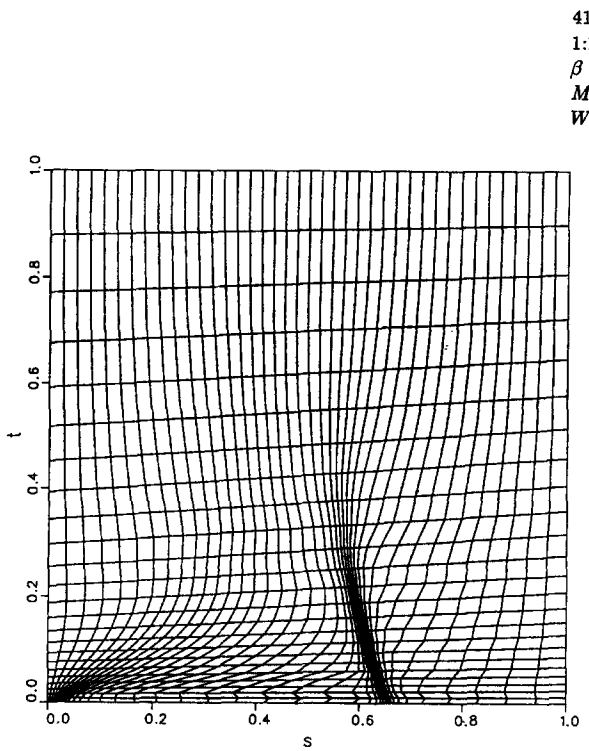

Fig. 23. Adapted reference grid — 3rd adaptive iteration.

Fig. 19 shows the adapted physical space grid after the second adaptive iteration. Fig. 20 shows the adapted reference grid utilized to produce the adapted physical space grid. A gradient scaling factor $\beta = 1.0$ was used for the second adaptive iteration because the high gradient regions were much more clearly defined during the first adaptive iteration. As in the first adaptive iteration, the Mach number surface has undergone two smoothing iterations ($M_{\text{smooth}} = 2$) while the adaptive weight surface has undergone six smoothing iterations ($W_{\text{smooth}} = 6$). The second adapted grid (Fig. 19) shows that the grid lines are becoming more compressed in the vicinity of the shock wave. The resulting grid remains very smooth with good overall orthogonality. Fig. 21 shows the converged flowfield solution on the adapted grid after the second adaptive iteration. Notice that there is an overshoot due to the type of flow solver being used. Although Fig. 21 shows that the shock wave is slightly more defined within the field, there is not much improvement in shock resolution on the airfoil surface over the first adaptive iteration (Fig. 18).

Fig. 22 shows the adapted physical space grid after the third adaptive iteration. Fig. 23 shows the adapted reference grid utilized to produce the adapted physical space grid. As in the second adaptive iteration, a gradient scaling factor $\beta = 1.0$, $M_{\text{smooth}} = 2$, and $W_{\text{smooth}} = 6$ were utilized. The third adapted grid (Fig. 22) shows even more grid line compression in the vicinity of the shock wave, while retaining very smooth grid line variations with good overall orthogonality. Fig. 24 shows the converged flowfield solution on the adapted grid after the third adaptive iteration.

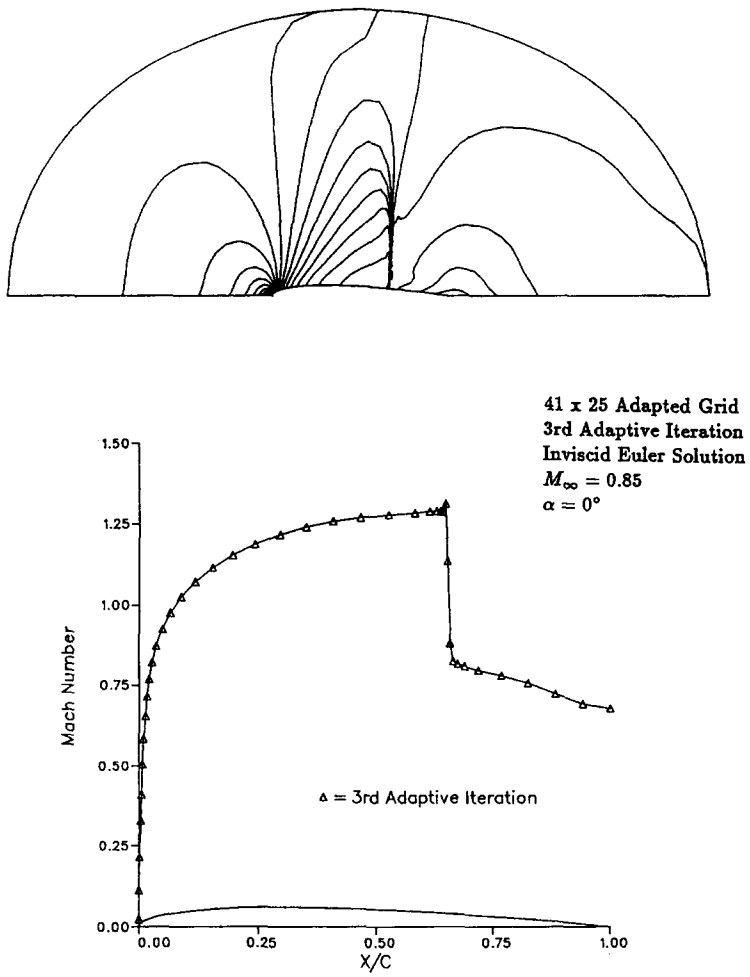

Fig. 24. Converged flowfield solution — 3rd adaptive iteration.

Again, Fig. 24 shows that there is some slight improvement in shock resolution within the field as compared to the previous iteration, but not much improvement on the surface solution.

Fig. 25 summarizes the improvement obtained by the solution adaptive grid procedure implemented in the present algorithm. Fig. 25 shows the improvement in grid resolution in the vicinity of the shock wave and subsequent improvement in the resolution of the shock wave discontinuity in the flow solution. Fig. 26 compares the Mach number distribution on the airfoil surface for the initial grid and the subsequent adaptive iterations. Fig. 26 shows that the shock is captured much sharper after just one adaptive iteration, and not much improvement in the second and third adaptive iterations. This result indicates that only one adaptive iteration is required to adequately resolve the shock wave on the airfoil surface for this particular problem.

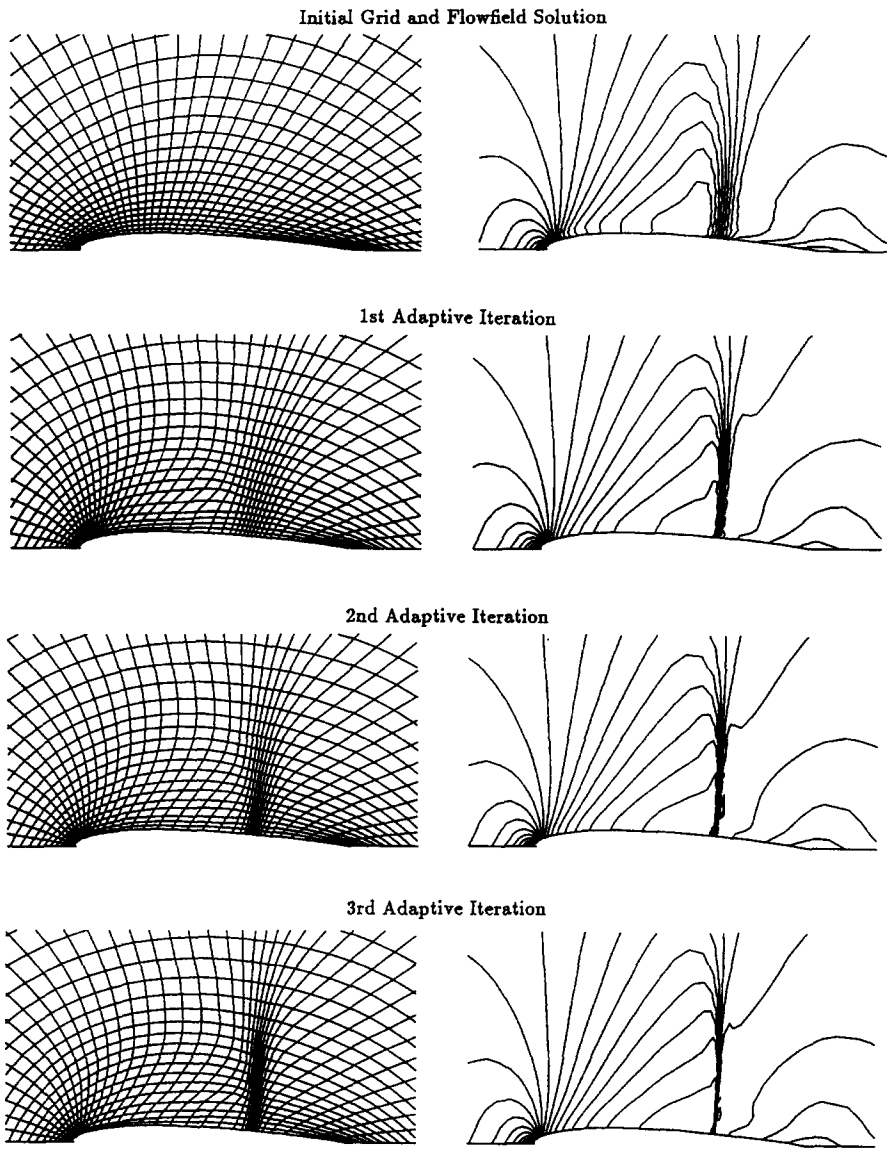

Fig. 25. Comparison of the nearfield grids and Mach contours.

6. Conclusions

In the present study, the discrete variational (DV) grid generation method has been used to produce grids suitable for solving the inviscid Euler equations for transonic flow past an airfoil. Examples of O-type and C-type grid configurations around an airfoil demonstrate the capabilities of the DV method. Through the use of the reference grid, the DV method provides excellent control over grid line clustering in the interior of the grid while maintaining smoothly varying grid line distributions.

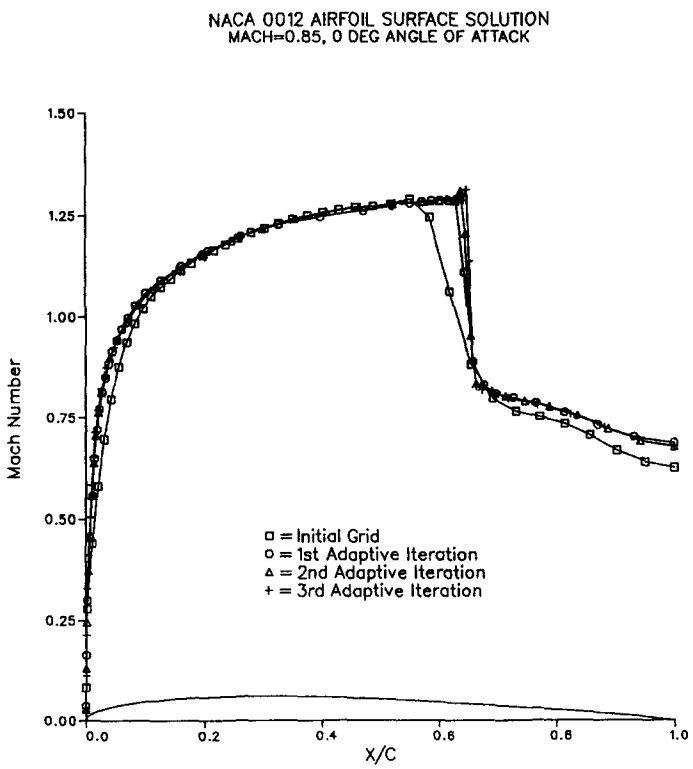

Fig. 26. Comparison of Mach number distributions on the airfoil surface.

The solution adaptive grid procedure implemented in the present algorithm has been shown to provide excellent control over grid line clustering in regions of high flow (solution) gradients while maintaining a smoothly varying grid line distribution over the field. The present formulation provides for a high degree of grid line clustering in high gradient regions without other regions becoming devoid of points. The improvement in shock wave resolution on the surface of the airfoil in transonic flow demonstrates the improvement obtainable with this solution adaptive procedure.

The DV grid generation method coupled with the solution adaptive grid procedure developed in the present study are combined to produce a powerful tool for generating solution-adaptive grids for improved flowfield analysis. Further studies are needed to determine in what situations this method may be superior. Another issue of importance is the convergence of the adaption itself. This issue will be addressed in our next paper. In particular extensions to three dimensions where the cost of the grid is crucial are under way.

References

[1] J.S. Abolhassani and R.E. Smith, Multiple-block grid adaption for an airplane geometry, in: *Proc. 2nd Internat. Conf. in Numerical Grid Generation in Computational Fluid Mechanics*, Miami Beach, FL (1988) 815–823.

[2] D.A. Anderson, Constructing adaptive grids with Poisson grid generators, in: *Proc. 1st Internat. Conf. in Numerical Grid Generation in Computational Fluid Dynamics* (1986) 125–136.
[3] R. Beam and R.F. Warming, An implicit finite difference algorithm for hyperbolic systems in conservation law form, *J. Comput. Phys.* **22**(1) (1976) 87–110.
[4] R.A. Benson and D.S. McRae, A three dimensional dynamic solution-adaptive mesh algorithm, AIAA Paper 90-1566, in: *AIAA 21st Fluid Dynamics, Plasma Dynamics, and Lasers Conf.*, Seattle, WA (1990).
[5] J.U. Brackbill and J.S. Saltzman, Adaptive zoning for singular problems in two dimensions, *J. Comput. Phys.* **46** (1982) 342–368.
[6] J.E. Castillo, A direct variational grid generation method, in: *Proc. 6th IMACS Inter. Symp. on Computer Methods for Partial Differential Equations*, Lehigh Univ., Bethlehem, PA (1987).
[7] J.E. Castillo, A discrete variational grid generation method, *SIAM J. Sci. Statist. Comput.* **12**(2) (1991) 454–468.
[8] J.E. Castillo, An adaptive direct variational grid generation method, *Comput. Math. Appl.* **21**(5) (1991) 57–64.
[9] J.E. Castillo, Direct optimization grid generation methods, in: *Proc. 14th IMACS World Congress on Computational and Applied Mathematics*, July 1994.
[10] J.E. Castillo, G. McDermott, M. McEachern and J. Richardson, A comparative analysis of numerical techniques applied to a model of the otolith membrane, *Comput. Math. Appl.* **24**(7) (1992) 133–141.
[11] J.E. Castillo and E.M. Pedersen, A solution adaptive algorithm for the discrete variational grid generation method, to be published.
[12] J.E. Castillo, S. Steinberg and P.J. Roache, On folding of numerically generated grids: Use of a reference grid, *Comm. Appl. Numer. Methods* **4** (1988) 471–481.
[13] G.K. Cooper and J.R. Sirbaugh, PARC code: Theory and usage, AEDC-TR-89-15, Arnold Engineering Development Center, Arnold Air Force Base, TN, 1989.
[14] A.D. Harvey, S. Acharya, S.L. Lawrence and S. Cheung, A solution adaptive grid procedure for an upwind parabolized flow solver, AIAA Paper 90-1567, in: *AIAA 21st Fluid Dynamics, Plasma Dynamics, and Lasers Conf.*, Seattle, WA (1990).
[15] C. Hsiufang, Solving a large scale optimization problem arising from grid generation, Technical Report SDSU.IRC.4.91, San Diego State University (1991).
[16] S.R. Kennon and G.S. Dulakravich, A posteriory optimization of computational grids, AIAA paper No. 85-0483, in: *AIAA 23rd Aerospace Science Meeting*, Reno, NV (1985).
[17] H.J. Kim and J. Thompson, Three dimensional adaptive grid generation on a composite block grid, AIAA Paper 88-0311, in: *AIAA 26th Aerospace Sciences Meeting*, Reno, NV (1988).
[18] P. Knupp and S. Steinberg, *Fundamentals of Grid Generation* (CRC Press, Boca Raton, FL, 1993).
[19] K.D. Lee, J.M. Loellbach and T.R. Pierce, Solution adaptive grid generation using a parametric mapping, in: *Proc. 2nd Internat. Conf. in Numerical Grid Generation in Computational Fluid Mechanics*, Miami Beach, FL (1988) 455–464.
[20] K.D. Lee, J.M. Loellbach and M.S. Kim, Adaption of structured grids for improved Navier–Stokes solutions, AIAA Paper 90-0125, in: *AIAA 28th Aerospace Sciences Meeting*, Reno, NV (1990).
[21] E.M. Pedersen, Solution adaptive grid generation for fluid flow calculations using the discrete variational grid generation method, Master's Thesis, San Diego State University (1992).
[22] T.H. Pulliam, Euler and thin layer Navier–Stokes codes: ARC2D, ARC3D, *Notes for Computational Fluid Dynamics Users' Workshop*, University of Tennessee Space Institute, Tullahoma, TN (UTSI Publication E02-4005-023-84) (1984) 15.1–15.85.
[23] P.J. Roache, K. Salari and S. Steinberg, Hybrid adaptive Poisson grid generation and grid smoothness, *Comm. Appl. Numer. Methods* **7** (1991) 345–354.
[24] P.J. Roache and S. Steinberg, A new approach to grid generation using a variational formulation, AIAA Paper 85-1527, in: *AIAA 7th Computational Fluid Dynamics Conf.*, Cincinnati, OH (1985).
[25] W. Shyy, An adaptive grid method for Navier–Stokes flow computation, *Appl. Math. Comput.* **21** (1987) 201–219.
[26] J.F. Thompson, F.C. Thames and C.W. Mastin, Automatic numerical generation of body-fitted curvilinear coordinate systems for field containing any number of arbitrary two-dimensional bodies, *J. Comput. Phys.* **15** (1974) 299–319.